EXAMINATION OF *P/S* SPECTRAL RATIOS FOR SMALL EXPLOSIONS AT LOCAL DISTANCES AND INTERPRETATION OF MOMENT TENSORS ESTIMATED FROM NEAR-SOURCE DATA

Mark R. Leidig[1], Brian W. Stump[2], William R. Walter[3], Anastasia F. Stroujkova[1], Xiaoning Yang[4], and Jessie L. Bonner[1]

Weston Geophysical Corp.[1], Southern Methodist University[2], Lawrence Livermore National Laboratory[3], and Los Alamos National Laboratory[4]

Sponsored by the National Nuclear Security Administration

Contract Nos. DE-AC52-08NA28655[1,2], DE-AC52-07NA27344[3], and DE-AC52-06NA25396[4]
Proposal No. BAA08-97

ABSTRACT

The ratio of 6-8 Hz *P/S* energy is a robust discriminant between earthquakes and explosions at regional distances (e.g., Taylor et al., 1989; Walter et al., 1995; Hartse et al., 1997; Pasyanos et al., 2009). We have examined the *P/S* discriminant at regional and local distances for simultaneously-detonated chemical explosions conducted for the Non-Proliferation Experiment (NPE), Source Phenomenology Experiments in Arizona (SPE Black Mesa and Morenci), Alaska Frozen Rock Experiments (FRE Frozen and Unfrozen), the New England Damage Experiment (NEDE) and other datasets. The shots were conducted at various scaled depths of burial in lithologies ranging from granite to alluvium. Several of these datasets have delay-fired mining explosions detonated in close proximity to the dedicated shots for comparison.

At regional distances, the discrimination analysis includes identifying and picking the onset times of the local and regional phases *Pn*, *Pg*, and *Lg*, making amplitude measurements in a variety of passbands, normalizing those measurements for the effects of source and path using the Magnitude and Distance Amplitude Correction (MDAC) methodology (Walter and Taylor, 2002), and calculating *P/S* ratios for each event. We find that the MDAC-corrected SPE Black Mesa ratios fall in the middle of the nuclear explosion population at station KNB with very little variation due to the differing shot conditions.

At local distances, we windowed the *P*- and *S*-waves based on travel times and particle motion. We then estimated smoothed spectra for the *P*- and *S*-waves and formed *P/S* spectral ratios. The signal quality and difficulty in picking the shear arrival varied between the data sets. The NEDE dataset had the best *S*-wave development, while other datasets were complicated by *P*-coda, small amplitude shear-wave generation, and additional arrivals that were not shear waves based on velocity and polarization analyses. Some of the variability in the *P/S* results could be related to error in the phase picking and analysis.

We typically observed larger *P/S* ratios for confined shots than free-face shots. We also observed larger *P/S* ratios for the NEDE Comp B shots than with ANFO shots. There are a number of interesting and unexplained results including: a) well defined shear waves from the NEDE compared to the other experiments, b) large variations in ratios with distance for SPE Black Mesa Shot 1 and the NEDE black powder shot, c) FRE having the largest ratios at certain distances and near smallest at others, d) the FRE frozen rock shot ratios not consistently larger than the unfrozen rock shots, and e) some well-confined Morenci shots having ratios similar to free-face shots. We plan to address these issues during the final year of this project.

The resolution of moment tensors determined using near-source observations is dependent upon the observations, the propagation path model and source model assumptions. Moment tensors determined from the inversion of near-source data generated by a contained single-fired explosion conducted at SPE Morenci (copper mine) document a strong Compensated Linear Vector Dipole (CLVD) contribution. A set of numerical tests are reviewed that assess the uniqueness of this source interpretation.

OBJECTIVES

We continue to study the physical mechanisms for shear wave generation from small chemical explosions. We are conducting moment tensor inversions and analyzing regional and local distance *P/S* ratios for a variety of different explosion experiments relative to normal production mining explosions, natural earthquakes, and previous nuclear tests at the Nevada Test Site.

RESEARCH ACCOMPLISHED

Interpretation of Near-Source Moment Tensor Inversions

The resolution of the seismic source is dependent upon the source model parameterization, the observational data and propagation path effects. The Source Phenomenology Experiment (SPE) conducted a series of single-fired experiments in a copper mine in Arizona (Morenci) and a coal mine in Arizona (Black Mesa) providing the opportunity to investigate the source characterization of explosions and address the resolution of the source. Here we discuss some of the resolution issues as investigated through source inversions of the copper mine explosions focusing on the effects of observational data and a complementary synthtic study focusing on the importance of the source parameterization. Critical to these studies is the establishment of the importance of isotropic versus nonisotropic source contributions with a goal of improved understanding of *S*-wave generation from explosions.

Zhou et al. (2005) report on moment tensor inversions for a number of the single-fired explosions as part of SPE Morenci showing both the effects of assumed propagation path model as well as the distribution of stations observing the source. One of these moment tensor inversions is summarized below where 8 three-component records from a variety of azimuths (~180^{o} coverage) and distance ranges (~150 to 700 m) were utilized in an inversion for the moment tensor for a contained explosion with a total explosive weight of 13,600 lbs and a scaled depth of 127 m/kt$^{1/3}$ (SPE Morenci Shot 10). The moment tensor that was estimated for this explosion is reproduced in Figure 1. It illustrates the strong contribution from the diagonal elements of the moment tensor characteristic of an explosion but also includes an enhanced M_{zz} component with the ratio of M_{xx}:M_{yy}:M_{zz} approximately 1:1:2 characteristic of a CLVD. This ratio and the relative size of the moment estimates were insensitive to choices of stations used in the inversion. The condition number (Figure 1) from the inversion provides a measure of the adequacy of the station distribution for unique recovery of all elements of the moment tensor as a function of frequency. Typically condition numbers below 100 are satisfactory. The physical interpretation of this source and the uniqueness of the interpretation are further illustrated with some simple numerical experiments reported next.

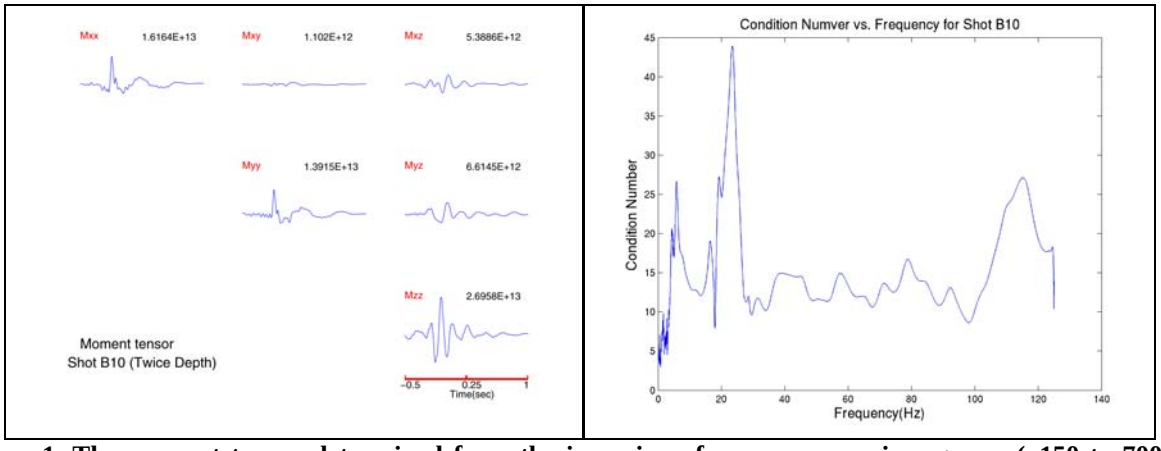

Figure 1. The moment tensor determined from the inversion of near-source seismograms (~150 to 700 m) from Shot B10 (13,600 lbs and scaled depth of 127 m/kt$^{1/3}$) is displayed on the left. The condition number from the inversion is plotted versus frequency in the right figure.

A number of physical models of the source have been proposed for the estimated moment tensor asymmetry documented including the effect of near-surface spallation and more broadly the interaction of the explosion stress waves with the region above the detonation point. The interpretation of the resulting moment tensor is dependent

upon the uniqueness of the moment tensor representation, the resolution of the individual elements of the moment tensor and the importance of assumed source depth in these source inversions.

Spallation that accompanies explosions detonated near the free surface can result from the tensile failure of the near surface layers above the source. This nonlinear failure can re-partition the initially symmetric wave field into waves indicative of cylindrical symmetry. This secondary source can be represented by a set of vertical forces that are applied at a shallower depth than the initial explosion. A set of numerical tests was conducted to illuminate these effects and their relationship to the moment tensor representation. These tests were designed to replicate a contained explosion at a depth of 11.5 m (253 lbs yield) with observations from 50 to 150 m, somewhat similar to the depths and ranges in the SPE inversions. The spallation source was computed for a depth of 3 m. Figure 2 illustrates the similarity of radiated vertical waveforms from the vertical force and waveforms generated by a CLVD. Except for a difference of one temporal differential, the point force and CLVD sources produce very similar waveforms in an elastic half space even with their differences in depth. Comparison of both the radial and vertical synthtics for the two sources produce similar relative amplitudes and decays over a range of distances as demonstrated in Figure 2.

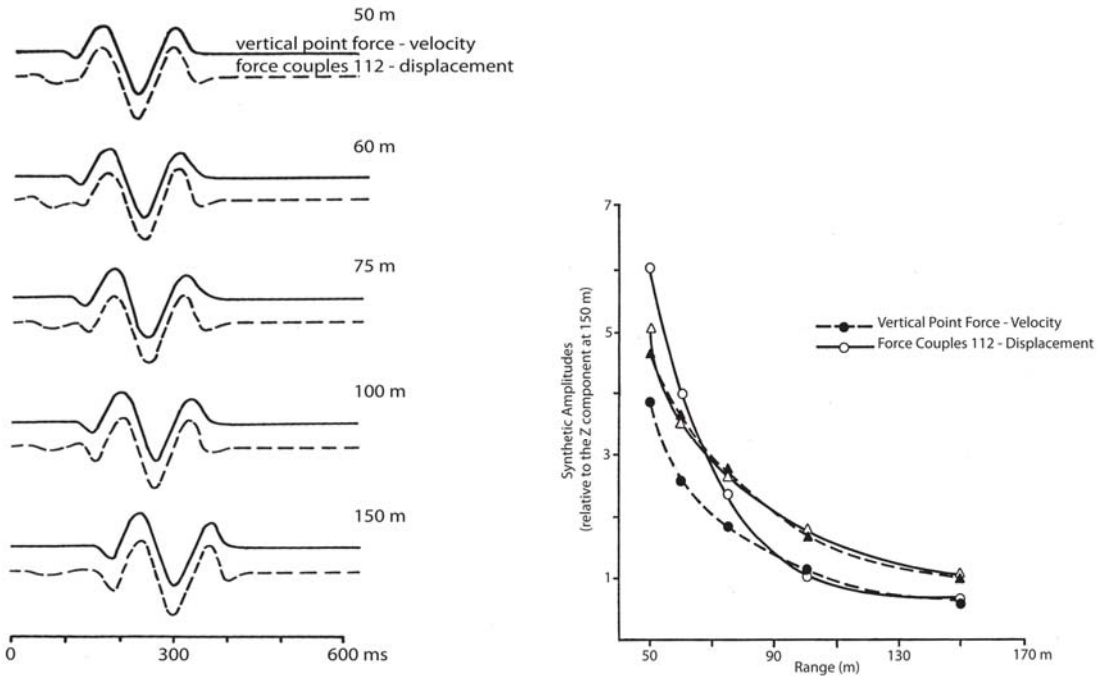

Figure 2. (Left) Comparison of vertical velocity from a vertical point force source at 3m in an elastic half-space to the vertical displacement from a CLVD at 11.5 m illustrating the similarity of waveforms. (Right) The spatial decay of the vertical and radial velocity from the vertical point force and the vertical and radial displacement from the CLVD over the distance range of 50 to 150 m.

These synthetic comparisons illustrate the great similarity of waveforms expected from a CLVD and vertical force source model. They reflect a linearity between the two models that must be taken into account when either completing source inversions or interpreting the resulting representation. As noted earlier, the condition number of moment tensor inversions is one way to quantify these interactions. A set of synthetic seismograms was produced combining a spall source at 3 m and an isotropic explosion at 11.5 m. An inversion that included the moment tensor plus vertical point force was compared to an inversion in which the source was represented only as a moment tensor. The condition numbers for these two inversions are replicated in Figure 3 and illustrates that the strong linearity between the vertical point source and the CLVD results in large condition numbers when the point force is included.

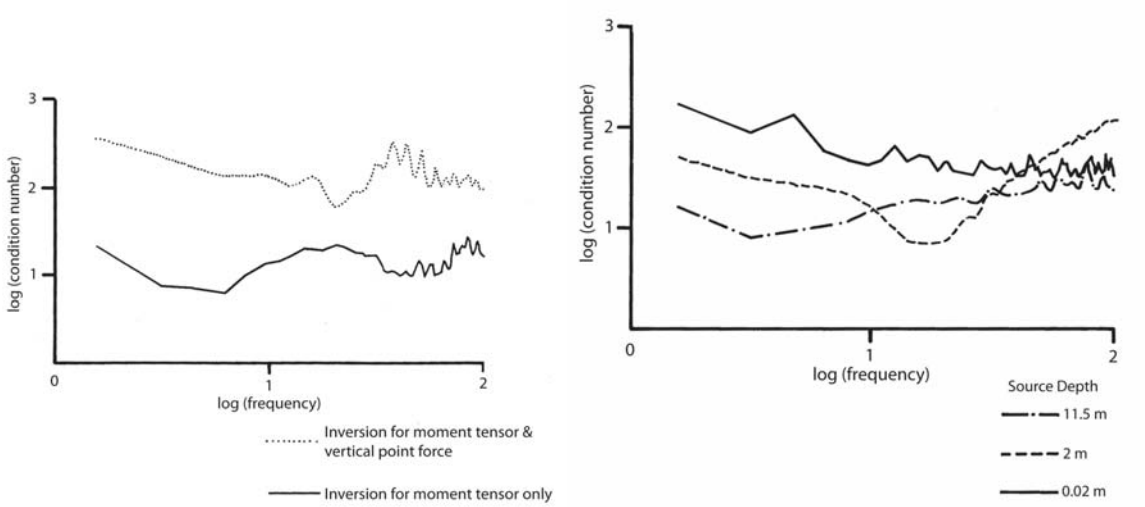

Figure 3. (Left) Condition numbers from a synthetic inversion that includes a moment tensor plus vertical point source representation and an inversion that is represented by only a moment tensors. (Right) Condition numbers for moment tensor inversions with source depths from 11.5 to 0.02 m.

One final synthetic test illustrates additional considerations when conducting near-source moment tensor inversions, the assumption of source depth. As shown earlier in the synthetic waveform comparison (Figure 2), possible differences in source depth for different parts of the source representation may be difficult to resolve with near-source data. As the depth of the source becomes shallower, there is additional non-uniqueness introduced by the free surface. Figure 3 reproduces the condition numbers for a series of near-surface (50 to 150 m range observation) moment tensor inversions at ever-shallower depths. A general increase in condition number with frequency and decreasing source depth documents the problem in fully resolving the moment tensor for shallow explosions.

In conclusion, moment tensor inversions from the SPE explosions detonated in a copper mine show a strong CLVD contribution. Inversions with different distributions of observations suggest that this contribution is not affected by station distribution. Synthetic tests are consistent with this source resulting from a spall contribution although depth resolution of this secondary source may affect a unique physical interpretation of the source. Secondary sources with very shallow depths, especially as they approach the free surface, may be difficult to resolve as indicated by the synthetic tests. Work still remains to be completed to address trade-offs between the assumed propagation path effects and the resulting moment tensors.

Regional Distance *P/S* Ratios

We have examined the behavior of regional discriminants from the Arizona SPE. The discrimination analysis includes identifying and picking the onset times of the local and regional phases *Pn*, *Pg*, and *Lg*, making amplitude measurements in a variety of passbands, normalizing those measurements for the effects of source and path using the MDAC methodology (Walter and Taylor, 2002), and calculating *P/S* ratios for each event. Figure 4 shows the 6-8 Hz *Pg/Lg* ratio results at station KNB (Kanab, Utah) for six of the Black Mesa coal mine SPE shots (diamonds) and production mining explosions (triangles), compared to a set of nuclear tests (stars) and western U.S. earthquakes (circles). We find that the MDAC-corrected production explosions and SPE shots at Black Mesa fall in the middle of the nuclear explosion population with very little variation due to the differing shot conditions. Thus for this particular discriminant at this station, the SPE shots and mining explosions are good surrogates for nuclear explosions, and the differences in depth of burial and single versus multiple shot have only a small effect on the discriminant measures.

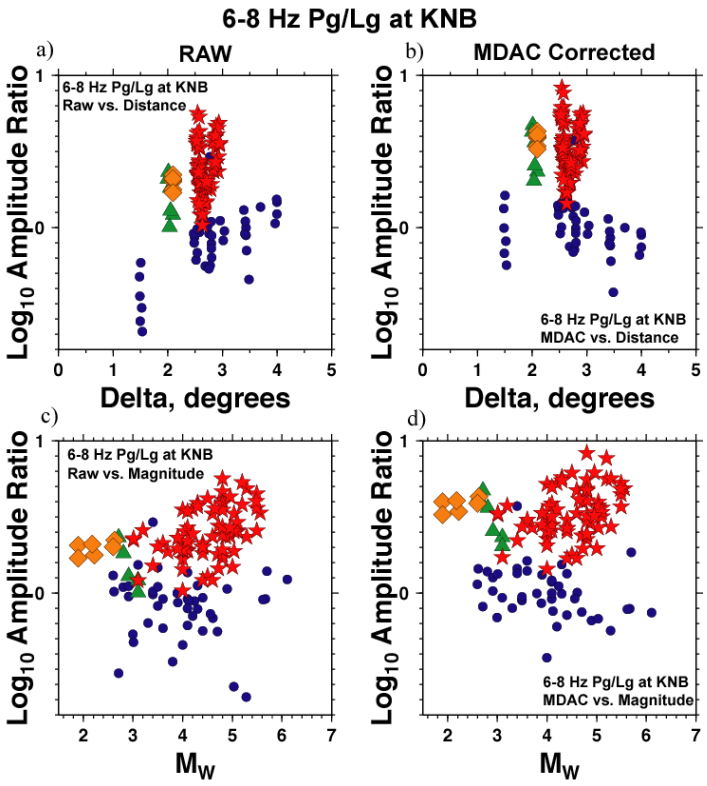

Figure 4. Comparison of six SPE shots from the Black Mesa coal mine (diamonds) with production shots at the same mine (triangles) at station KNB using the 6-8 Hz *Pg/Lg* discriminant (e.g. Walter *et al.*, 1995). The ratios are plotted as either raw (a and c) or MDAC-corrected (b and d) amplitude ratios as a function of distance (a and b) or moment magnitude (c and d). The SPE shots show low variability and have similar values to the mean of the nuclear tests (stars), making them possible surrogates in this discriminant case. Earthquakes are plotted as circles.

Local Distances *P/S* Ratios

Data. We have examined the *P/S* ratios at local distances for simultaneously-detonated chemical explosions conducted for the SPE Morenci and Black Mesa (Bonner et al., 2005), Alaska Frozen Rock Experiments (FRE Frozen and Unfrozen; Bonner et al., 2009), the New England Damage Experiment (NEDE; Leidig et al., 2010) and other datasets. The shots were conducted at various scaled depths of burial in lithologies ranging from granite to alluvium. Several of these datasets have delay-fired mining explosions detonated in close proximity to the dedicated shots for comparison.

Processing. To compare *P* and *S* amplitudes we processed data from the 3-component stations that recorded each of these explosion experiments at local distances. We used remote stations (> 5 km) because *S* and *Rg* phases are not well-separated at distances less than a few kilometers. The initial part of the data processing included correction for the instrument response. The next step in the data processing is identifying *S*-waves. It was done by studying the apparent velocity of the phase (moveout) and the particle motion for the 3C stations. Figure 5 shows the particle motions for NEDE Shot 4 at station SE02 (6 km). At this distance the *S* arrival is separated from the *Rg* phase, which dominates the waveforms at shorter distances. The *P*-wave arrival is polarized approximately parallel to the propagation azimuth. The arrival in the presumed *S*-window in question is polarized approximately perpendicular to the propagation azimuth suggesting that this is indeed an *S* wave.

Signal Quality. The signal quality and difficulty in picking the shear arrival varied between the data sets. The NEDE dataset had the best *S*-wave development, especially at SE02 (Figure 5). The *P* and *S* arrivals are easy to identify in the waveforms and the particle motions show more classic *P* and *S* motion than for the other experiments.

For the SPE data, distinct *S* arrivals were difficult to identify in the waveforms. The *S* windows had little transverse motion, but considerable radial motion indicating possible contamination by *P* coda. Both the SPE Morenci and Black Mesa recordings contained many arrivals other than the simple *P*, *S*, and surface waves. These arrivals could be reflected or refracted *P* waves, but regardless, they make *S* identification more difficult and add noise to the shear wave window.

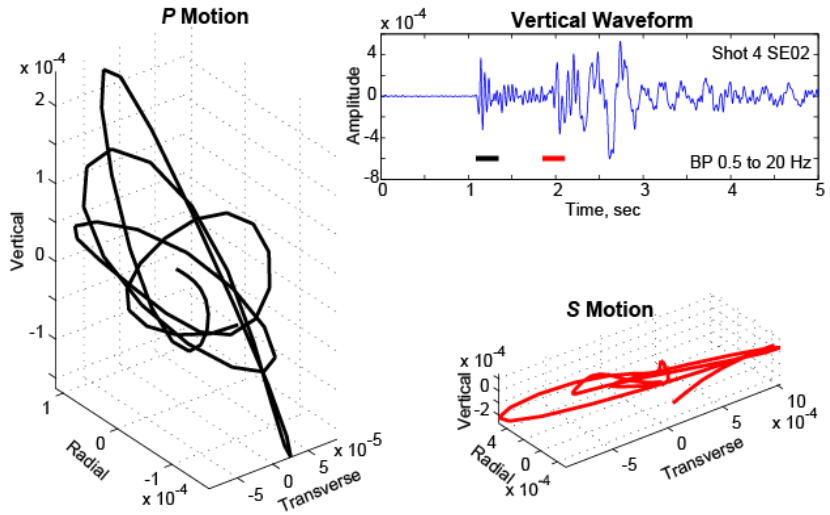

Figure 5. Seismogram (top right) and particle motion plots (left and bottom right) for NEDE Shot 4 records at station SE02.

The *S* waves from the FRE frozen rock shots were extremely difficult to observe in the waveforms, while they were easier to identify from the unfrozen FRE rock shots. The low amplitude *S* window motions resemble *P* motions and again may indicate *P* coda contamination. An interesting arrival only on the transverse component was noted at one station. The arrival came in prior to the expected *S* arrival and could possibly be a *P*-to-*S* conversion somewhere along the travel path.

***P/S* Spectral Ratios.** Once the *P* and *S* windowing were complete, a power spectral density (PSD) using Welch's method was calculated on *P*, *S*, and noise windows from the vertical component. Ratios were then formed using the smoothed spectra. Examination of *P/S* spectral ratios was conducted using equal event-to-station distances to compare different emplacement media. Shot 3 from the Morenci SPE, Shot 7 from the Black Mesa SPE, Shots 2 and 5 from the FRE, and Shot 4 from the NEDE were chosen for comparison as each used ANFO and had similar yields and emplacement depths. Stations at similar distances of 6 and 12 km from each shot were used (Table 1).

Figure 6 shows that the *P/S* spectral ratios at distances of 6 km and 12 km have interesting differences and similarities. For measurements on stations at ~6 km, the ratios are near or below 1 for frequencies below 10 Hz and then gradually build to peak around 30 Hz, except for the Black Mesa curve which peaks at 50 Hz. At 12 km distance, there is a large range of peak ratio frequencies ranging from 9 to 40 Hz. As at 6 km, the Black Mesa shot has the largest peak *P/S* ratio and the NEDE shot has the smallest ratio. The spectra of the two FRE shots have a similar shape, but have a frequency shift with the frozen rock shot peaking at a higher frequency.

In addition, we examined the *P/S* ratios in discrete frequency bands of 1-2, 2-4, 4-8, and 8-16 Hz for all shots and experiments. The ratios were excluded from analysis if the spectra or waveforms were suspected of being affected by the background noise or other 'foreign' signal. Therefore not every shot is represented at every distance. Distances of 6, 12, and 24 km were examined for each experiment. There was not a station near 24 km distance for Black Mesa SPE, so a station at 34 km distance was used. Table 1 lists the stations used and their average distances.

The ratios were compared for each shot as a function of frequency, distance, and yield. The *P/S* ratios in the following plots are color coded by experiment (Table 2) and the symbol shape represents the experiment shot number (Table 3). Note that the Morenci Shot 9 did not detonate so Shot 10 is given the Shot 9 symbol.

Table 1. Analyzed Stations and Distances (km)

SPE Morenci		SPE Black Mesa		FRE		NEDE	
MR02	6.1	L3A	4.7	MDR	5.5	SE02	6.0
MR04	12.1	NN24	13.9	PED	13	SE04	12.2
MR08	25.1	NN23	34.5	ALPAF	22.3	SE08	23.7

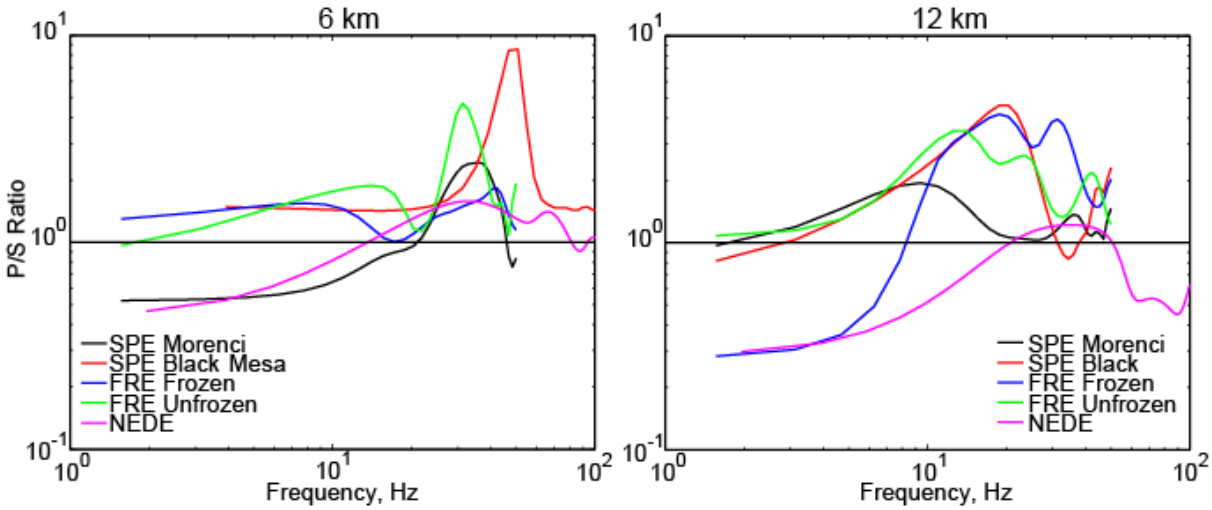

Figure 6. Spectral ratios at equidistant stations of a) 6 km and b) 12 km for the different explosion experiments.

Table 2. Experiment Color Legend

Experiment	Symbol Color
SPE Morenci	Black
SPE Black Mesa	Red
FRE	Blue
NEDE	Green

Table 3. Shot Symbol Legend

Shot #	Symbol
1	+
2	O
3	*
4	□
5	◊
6	△
7	▽
8	☆
9/10	◁

***P/S* Ratio versus Distance.** Figure 7 plots the discrete frequency band *P/S* ratios as a function of distance. At 6 km distance, all ratios are greater than 0.9. The smallest ratios (0.3) and the largest spread of ratios are observed at 12 km distance. By 24/34 km, the scatter is reduced and the minimum ratio value has increased to 0.5. The FRE ratios decrease with distance, while the NEDE ratios decrease from 6 to 12 km but increase out to 24 km. The SPE Black Mesa ratios have a similar characteristic, except they are almost equal amplitude at all distances in the 8 to 16 Hz range. The Morenci ratios show the least variation across the distance ranges. At each distance, the NEDE ratios are typically the smallest. As noted previously, this data set had the most distinct shear wave arrivals, which may explain this observation. At 6 and 12 km, the FRE data set has some of the largest *P/S* ratios, but Morenci shots have the largest ratio at 24 km.

When comparing individual shots in each data set, it is observed that Shots 8 and 5 (2x burden shots) had the largest *P/S* ratios for SPE Morenci. Shots 2, 4, 6, and 7 (free-face and 2x depth shots) had the lowest ratios. Except for the 2x depth shots, these results are not surprising. The SPE Black Mesa shot ratios are tightly packed, with the

exclusion of Shot 1. Shots 8 and 9 (free-face shots) routinely show up near the bottom of the ratios, but this is not consistent and the difference is small. SPE Black Mesa Shot 1 is peculiar. This blast was conducted in a straight line of boreholes detonated near-simultaneously. The *P/S* ratio is at least 50% larger than the other SPE Black Mesa ratios at 6 km, but is barely half the size of the other ratios at 12 km. By 34 km, the ratio is indistinguishable from the other shots. Since this shot least resembled a point source, it is possible that a phase radiation pattern was generated and the station azimuth is affecting the ratios.

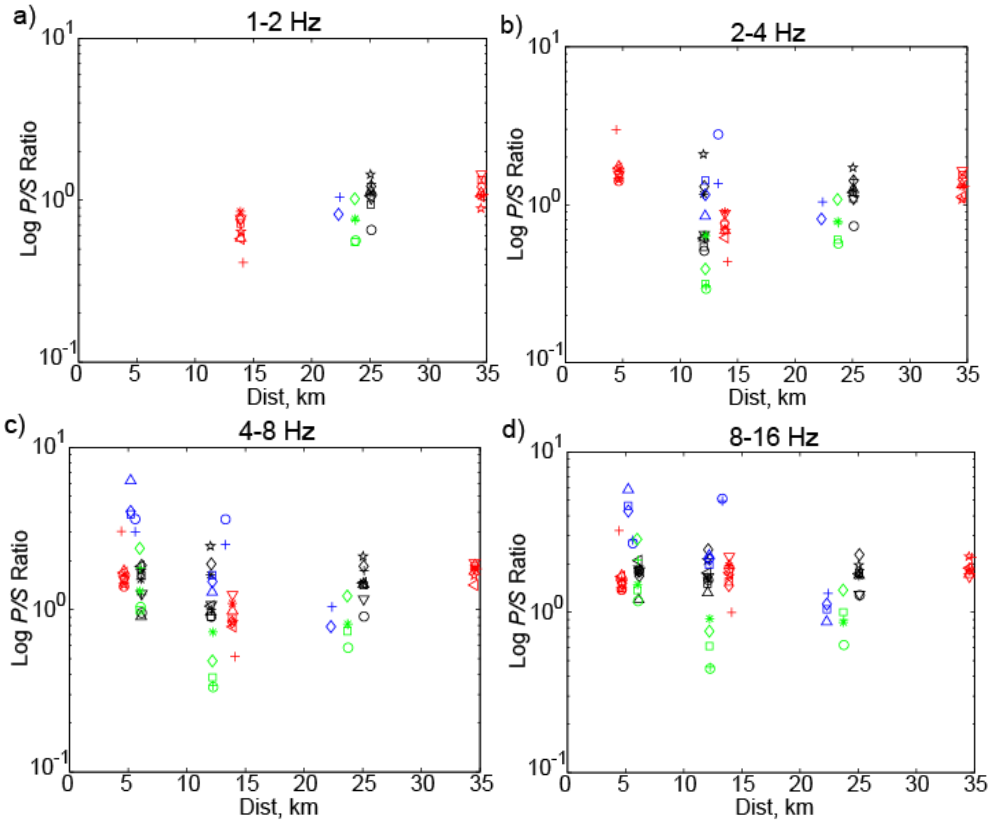

Figure 7. *P/S* spectral ratio as a function of distance. a) 1-2 Hz, b) 2-4 Hz, c) 4-8 Hz, d) 8-16 Hz. The data key is provided in Tables 2 and 3.

At 6 km distance, the FRE unfrozen rock shots have larger ratios (the largest ratios observed for all experiments), but elsewhere the frozen rock shots have larger ratios. The cause of this change is unclear but may be related to the near- source topography. The unfrozen rock shots and the MDR station near 6 km were located on a topographic high, while the frozen rock shots were detonated in a valley below. The ratios at the further stations may have been less affected by the topographic variations. There is not a clear relationship between shot size and *P/S* ratio within either group of frozen and unfrozen rock shots.

The NEDE Comp B shots exhibit the largest *P/S* ratios for that experiment with Shot 5 the largest at 6 and 24 km and Shot 3 the largest at 12 km. The NEDE ANFO Shots 2 and 4 have the smallest ratios at all distances and for all experiments. Shot 2 typically has the smallest ratio. The ratios for these two explosive types of shots behave exactly as anticipated and documented in previous work (Leidig et al., 2009). The Comp B shots lacked the shear wave generating fractures and therefore have a large *P/S* ratio. The NEDE black powder shot has peculiar behavior with distance though. At 6 km distance the ratio is large, at 12 km distance the ratio is similar to that of ANFO Shot 2 as the smallest, and finally at 24 km the ratio equals that of the Comp B Shot 3. However, the black powder shot was very deficient in high frequency energy as evidenced by near-source acceleration recordings.

***P/S* Ratio versus Frequency**. In Figure 8, the ratios are plotted as a function of frequency. A lack of temporal phase separation at the closer stations required shorter phase time windows which reduced the amount of data available in

the 1-2 and 2-4 Hz ranges. The ratios show a clear increase with frequency, particularly at 12 and 24 km distance. The scatter in the ratios is greatly reduced at 24/34 km distance. At this distance the two SPE data sets overlap, while the FRE and NEDE data sets overlap at slightly reduced ratios. At 12 km, FRE has the largest ratios, followed by the overlapped SPE data sets, and finally the NEDE ratios. The changes in ratio order with distance indicate the travel path and/or near receiver effects control the *P/S* ratio more than frequency, and this may provide evidence of shear wave generation away from the source. The frequency ranges at 6 km distance show overlapped ratios for SPE Morenci, SPE Black Mesa, and the NEDE, while the FRE ratios are distinctly larger.

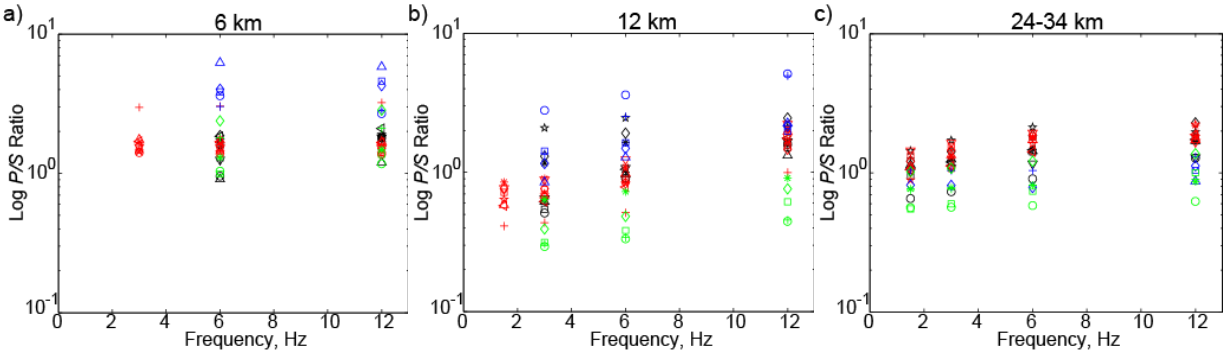

Figure 8. *P/S* spectral ratio as a function of frequency. a) 6 km, b) 12 km, c) 24/34 km. The data key is provided in Tables 2 and 3.

***P/S* Ratio of Single-Fired versus Delay-Fired Shots**. The *P/S* ratios of delay-fired mining blasts were also examined. Partial documentation of 8 production blasts at Morenci was obtained and 3 of these shots were examined. Documentation of 40 production shots at SPE Black Mesa was obtained. Only a handful of these events were recorded by the experiment equipment due to limited installation dates. Most of these shots had very small yield per 8 msec delay and resulted in very noisy recordings not suited for this analysis. Some of the larger yield/delay shots were near simultaneously detonated with other shots resulting in contaminated signals. Only one event was recorded on both L3A and NN24 with good signal-to-noise ratio.

The production shots were not conducted in the same test pits as the experiment explosions which created variations in distance and travel path. For example, station L3A was about 6 km from the SPE Black Mesa single-fired shots, but was more than 12 km from the production shot. Station NN24, which was around 14 km from the SPE blasts, was only about 8 km from the production shot.

Figure 9 plots the SPE single- and delay-fired blasts as a function of distance. Tables 2 and 3 apply to these plots except blue symbols are the Morenci production shots and green symbols are the SPE Black Mesa production shots. The most obvious difference in the *P/S* ratios is that the production ratios are typically less than the experiment blast ratios. In fact, some of the ratios are up to an order of magnitude smaller. This is particularly true at the shorter distances as the production shot ratios increase with distance while the single-fired ratios are more consistent. By 24/34 km distance, it would be nearly impossible to discriminate a single-fired shot from a delay-fired shot using *P/S* ratios, which is consistent with the regional distance data presented in Figure 4. At distances less than 15 km, setting a ratio threshold of 0.8 would do a decent job discriminating the shot types. Between 8 and 16 Hz, this would work well, but the misclassification increases with decreasing frequency.

CONCLUSIONS AND RECOMMENDATIONS

We have finished the first stage of our analysis of local *P/S* ratios from many small explosions in different emplacement media. The next stage will include examining earthquakes at similar distances and adding additional mining explosions. The final results will then be compared with regional MDAC-corrected data for chemical and nuclear explosions, mining explosions, and earthquakes. The largest uncertainty in the local distance *P/S* analysis is the correct identification of the shear wave arrivals by the analyst. Rotated three-component waveforms, hodograms,

record sections, and theoretical arrival times were used to aid the analyst, but the difficulty in confidently identifying the arrival in the filtered waveforms may result in error.

Many of the *P/S* ratios behaved as would be expected, as we observed larger ratios for confined shots than free-face shots and larger ratios for the NEDE Comp B shots than the ANFO shots. There are a number of interesting and unexplained results including: a) well defined shear waves from the NEDE compared to the other experiments, b) large variations in ratios with distance for the linear Black Mesa Shot 1 and the NEDE black powder shot, c) FRE having the largest ratios at certain distances and near smallest at others, d) the FRE frozen rock shot ratios not consistently larger than the unfrozen rock shots, and e) some well-confined Morenci shots having ratios similar to free-face shots. We plan to address these issues during the final year of this project.

Moment tensor inversions suggest a CLVD as a possible major component of the SPE Morenci sources. Synthetic models indicate spall as an additional possible source mechanism component, although reduced depth resolution could reduce the uniqueness of the physical interpretation.

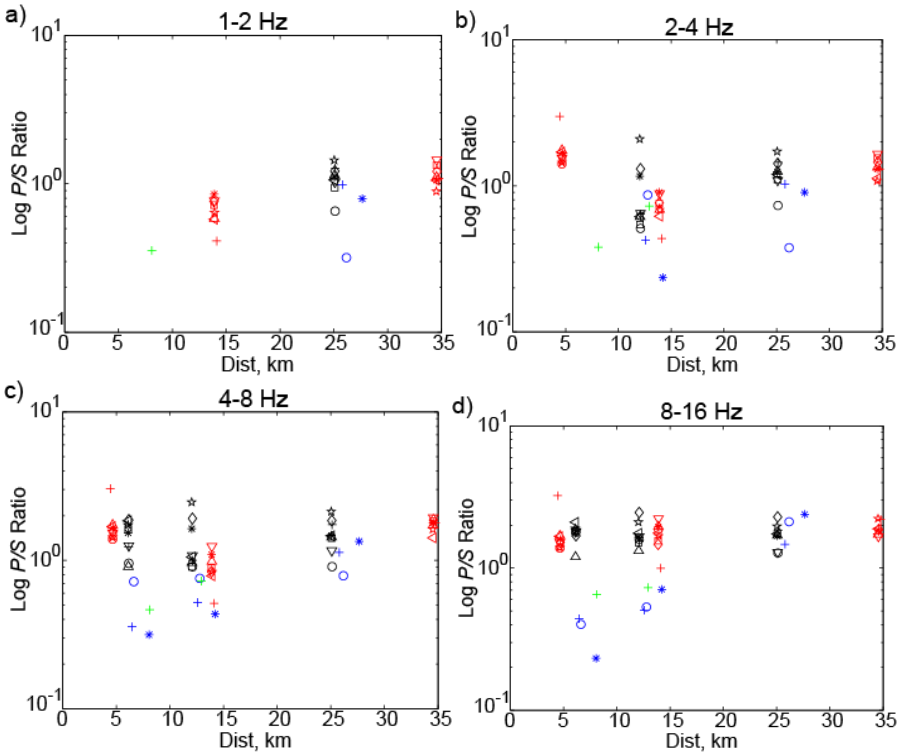

Figure 9. *P/S* spectral ratio as a function of distance for SPE planned and production shots. a) 1-2 Hz, b) 2-4 Hz, c) 4-8 Hz, d) 8-16 Hz. Figure key is shown in Tables 2 and 3, except blue symbols are Morenci production shots and green symbols are Black Mesa production shots.

REFERENCES

Bonner, J. L., B. Stump, M. Leidig, H. Hooper, X. Yang, R. Zhou, T. S. Kim, W. R. Walter, A. Velasco, C. Hayward, D. Baker, C. L. Edwards, S. Harder, T. Glenn, C. Zeiler, J. Britton, and J. F. Lewkowicz (2005). Source Phenomenology Experiments in Arizona, Weston Geophysical Corp. Final Report, 358 p.

Bonner, J. L., M. R. Leidig, C. Sammis, R.J. Martin (2009). Explosion coupling in frozen and unfrozen rock: experimental data collection and analysis. *Bull. Seism. Soc. Am.* 99**:** 830–851.

Hartse, H. E., S. R. Taylor, W. S. Scott, and G. E. Randall (1997). A preliminary study of regional seismic discrimination in central Asia with emphasis in western China, *Bull. Seismol. Soc. Am*. 87: 551–568.

Leidig, M., J. L. Bonner, T. Rath, and D. Murray (2010). Quantification of ground vibration differences from well-confined single-hole explosions with variable velocity of detonation, *Int. J. Rock Mech. Min. Sci.*, 47: 42–49.

Leidig, M., R. Martin, P. Boyd, J. Bonner, and A. Stroujkova (2009). Quantification of rock damage from small explosions and its effect on shear-wave generation: phase I—homogenous crystalline rock, in *Proceedings of the 2009 Monitoring Research Review*: *Ground-Based Nuclear Explosion Monitoring Technologies*, LA-UR-09-05276, Vol. 1, pp. 492–501.

Pasyanos, M. E., E. M. Matzel, W. R. Walter, and A. J. Rodgers (2009). Broadband *Lg* attenuation modeling in the Middle East, *Geophys. J. Int.* 177: *1166-1176, doi:10.1111/j.1365-246X.2009.04128.x.*

Taylor, S. R., M. D. Denny, E. S. Vergino, and R. E. Glaser (1989). Regional discrimination between NTS explosions and western U.S. earthquakes, *Bull. Seismol. Soc. Am.* 79: 1142–1176.

Walter, W. R., K. Mayeda, and H. J. Patton (1995). Phase and spectral ratio discrimination between NTS earthquakes and explosions, part 1: Emipirical observations, *Bull. Seismol. Soc. Am*. 85: 1050–1067.

Walter, W. R. and S. R. Taylor (2002). A revised Magnitude and Distance Amplitude Correction (MDAC2) procedure for regional seismic discriminants. Lawrence Livermore National Laboratory UCRL-ID-146882.

Zhou, R., B. W. Stump and X. Yang (2005). Moment tensor inversions of single-fired mining explosions at a copper mine in Arizona, *Eos Trans. AGU*, 86(52), Fall Meet. Suppl., Abstract S11B-0166.